HHS Public Access

Author manuscript

Nat Photonics. Author manuscript; available in PMC 2017 June 01.

Published in final edited form as:

Nat Photonics. 2016 December ; 10: 802–808. doi:10.1038/NPHOTON.2016.207.

High-magnification super-resolution FINCH microscopy using birefringent crystal lens interferometers

Nisan Siegel[1,2,3], **Vladimir Lupashin**[4], **Brian Storrie**[4], and **Gary Brooker**[1,2,3,*]

[1]Department of Biomedical Engineering, Johns Hopkins University, 9605 Medical Center Drive Suite 240, Rockville, Maryland 20850, USA.

[2]Microscopy Center, Johns Hopkins University Montgomery County Campus, Rockville, Maryland 20850, USA.

[3]CellOptic, Inc., 9605 Medical Center Drive Suite 224, Rockville, Maryland 20850, USA.

[4]Department of Physiology and Biophysics, University of Arkansas for Medical Science, 4301 West Markham Street, Little Rock, Arkansas 72205, USA.

Abstract

Fresnel incoherent correlation holography (FINCH) microscopy is a promising approach for high-resolution biological imaging but has so far been limited to use with low-magnification, low-numerical-aperture configurations. We report the use of in-line incoherent interferometers made from uniaxial birefringent α-barium borate (α-BBO) or calcite crystals that overcome the aberrations and distortions present with previous implementations that employed spatial light modulators or gradient refractive index lenses. FINCH microscopy incorporating these birefringent elements and high-numerical-aperture oil immersion objectives could outperform standard wide-field fluorescence microscopy, with, for example, a 149 nm lateral point spread function at a wavelength of 590 nm. Enhanced resolution was confirmed with sub-resolution fluorescent beads. Taking the Golgi apparatus as a biological example, three different proteins labelled with GFP and two other fluorescent dyes in HeLa cells were resolved with an image quality that is comparable to similar samples captured by structured illumination microscopy.

*Correspondence and requests for materials should be addressed to G.B. gbrooker@jhu.edu.

Author contributions

G.B. and N.S. designed and developed the concept for the birefringent lens interferometer and its implementation into the FINCH microscope, produced the hardware and software, conducted the FINCH and wide-field experiments and wrote the manuscript. V.L. prepared the HeLa cell immunolabelled fluorescent samples and took the image using the commercial SIM microscope shown in Supplementary Fig. 2. B.S. and V.L. provided various fluorescently labelled Golgi proteins in live cells and fixed samples during the course of this research that were important in the development of this new microscope. G.B. organized and supervised this work.

Additional information

Supplementary information is available in the online version of the paper.

Competing financial interests

The FINCH technology used in the study is owned by CellOptic, Inc. Additionally, this work was funded in part by CellOptic, Inc. G.B. is the founder of CellOptic, Inc., owns equity in the company and serves as the company's president and CEO. This arrangement has been reviewed and approved by the Johns Hopkins University in accordance with its conflict of interest policies. N.S. receives support from CellOptic, Inc. and B.S. is a consultant for CellOptic, Inc.

In classical optical imaging, an image is created from the light emitted or reflected by an object, without indexing the depths of the object points from which each image point originates. That is, the three-dimensional (3D) information about the object's shape is lost and only a 2D projection of the shape is recorded. Holography enables the imaging of the 3D information in a scene by recording interference fringes whose sizes and distributions are dependent on the exact 3D location of the object point from which the interfering light originates[1]. This property makes holography interesting for many applications, in particular fluorescence microscopy, as there is the potential to record 3D information about the object in question with many fewer exposures than are required at present. Current methods of holography mainly use coherent laser light to create holographic interference. Fluorescence light, however, poses a challenge for holography because it is incoherent. The ingenious development of scanning holography[2] overcame this limitation. An interferometer creates Fresnel interference patterns from laser light that are scanned across the sample to excite fluorescence that is ultimately correlated with the excitation beam to create a hologram. Another form of incoherent holography, FINCH, is an in-line motionless self-referenced holographic method[3–12] that can create an interferogram from the incoherent light (including fluorescent light) emitted or reflected from any object. Light originating from any point in the object is split into two beams that are differentially phase-modulated and recombined in a common plane to produce interference fringes. Another self-referenced incoherent holographic method[13] is based on dual beam path interferometers and thus does not have the simplicity and advantages of the FINCH in-line single-beam system. FINCH has the additional advantage of being inherently super-resolving, improving the lateral point spread function of classical imaging by a factor of 1.5–2. The challenge of implementing FINCH for fluorescence microscopy is to find ways to efficiently, and without optical aberrations, create self-interference of objects. The new all-optical single channel lens interferometers reported here for FINCH, made from birefringent crystals, resolve this issue, allowing optical imaging at a resolution beyond the Abbe limit even with high-numerical-aperture (NA) microscope objectives.

FINCH creates holograms from an object emitting incoherent light in a single-beam system by self-interference between two spherical waves originating from the object. A conceptual schematic of a FINCH microscope similar to that previously reported[8,9] is shown in Fig. 1, indicating an object emitting incoherent light at the front focal plane of an objective lens after epi-illumination. The emitted light propagates through the objective and a polarizing beamsplitter to an optical train that applies different spherical phases (focusing power) to different polarization components of the light beam, creating a pair of co-propagating differentially focused beams with focal lengths f_{d1} and f_{d2}. The beams propagate until their interference is recorded at the ideal hologram plane located at distance z_h, wherein the two beam sizes are the same. Following the recording of a set of holograms[3–12,14] used to recreate the complex field at the recording plane, a final processed image is calculated by Fresnel propagation[3,11] and a subsequent deconvolution.

One of the key parameters in the FINCH process is the relationship between the f_{d1} and f_{d2} and the optimal hologram recording plane at z_h. Holograms may be recorded at any point after the differential focus is applied, but the optimal hologram quality is achieved when the two waves obey the condition of maximal spatial overlap. The condition to ensure maximum

overlap between the f_{d1} and f_{d2} beams is met when the hologram is recorded in the plane at the distance z_h from the hologram-forming lens:

$$z_h = 2f_{d1}f_{d2}/(f_{d1}+f_{d2}) = (1+s)f_{d1} = (1-s)f_{d2} \quad (1)$$

where a spacing factor s obeys the equality:

$$s = |(f_{d2} - f_{d1})/(f_{d2}+f_{d1})| \quad (2)$$

As s (the relative distance between f_{d1} and f_{d2}) increases, the point hologram at plane z_h also increases in size, as described by the following equation:

$$R_H = sR_0 \quad (3)$$

where R_H is the aperture radius of the hologram and R_0 is the aperture radius of the wave at the spatial light modulator (SLM) or gradient refractive index (GRIN) lens or equivalent optic (such as the new birefringent lens system reported here) used to create the two concentric beams. This size increase renders the point hologram more easily resolvable by recording devices but decreases the average intensity of the hologram. There are other factors[7] that also establish upper and lower bounds for s. It is highly desirable to have independent control over z_h and s over a wide range to be able to optimize the holographic system for all possible variables. The z_h and s factors do not themselves change the resolution of the image coded by the hologram, but do affect the ease with which the hologram may be recorded, as well as other image factors such as magnification and depth of field.

In the past, our laboratory has demonstrated FINCH super-resolution in low-magnification, low-NA systems configured with SLM[6,7,10,11] and GRIN lens interferometers[8,9]. The SLM-based methods involve displaying one or more different lens patterns on an SLM and offer extensive flexibility in creating the desired z_h and s, but are prone to artefacts due to phase pattern sampling and digitization, as well as to lower light efficiency due to the loss of some light to higher-order diffracted images. Thus, fringe contrast can be reduced, leading to lowered contrast, resolution and signal-to-noise ratio in the final image. Since SLMs are reflective, the optical arrangement requires that the SLM be positioned at an angle to the optical axis of the imaging system[3,4,6,7,10–12], increasing optical aberrations even with corrected lens patters, or arranged on a beam splitter[5], decreasing the light budget. The GRIN-based FINCH system has improved the light budget and reduced artefacts, although it still produces characteristic artefacts and has little flexibility in the spacing factors available in a practical microscope configuration. It has therefore been desirable to identify other optics that can provide high-optical-quality polarized beamsplitting and non-aberrated differential focusing with flexible choice of focal lengths.

One possible method that could combine the advantages of the SLM and GRIN methods utilizes uniaxial birefringent crystals, which possess two different refractive indices, as the

material from which an otherwise standard spherical lens is constructed. If a birefringent refractive lens is cut so that the crystal's extraordinary axis lies in the plane orthogonal to the lens optical axis, the lens will possess two focal lengths, one each for the ordinary and extraordinary refractive indices n_o and n_e, as indicated in Fig. 2 and the thin-lens approximation of the lensmaker's equation as stated in equation (4):

$$f = R_{\text{eff}}/(n-1) \quad (4)$$

with f being the focal length of the lens, n the refractive index of the lens material and R_{eff} the effective curvature of the lens: $R_{\text{eff}} = R_1R_2/(R_1 + R_2)$ for a lens with two curved sides and $R_{\text{eff}} = R_1$ or $-R_2$ for a lens with one curved side; R_1 and R_2 are the radii of curvature of the two sides of the lens. Thus a single birefringent lens, made from birefringent material with n_o and n_e for the ordinary and extraordinary refractive indices, has focal length f_{bo} for light polarized along its ordinary axis and focal length f_{be} for light polarized along its extraordinary axis. These focal lengths may then be used to produce the f_{d1} and f_{d2} beams necessary for FINCH. As discussed in the Supplementary Information, a birefringent lens may be combined with standard lenses to obtain modified focal lengths f'_{bo} and f'_{be}, and thus enable independent control of z_h and s. For this work, a positively curved calcite lens was used on its own to produce a high spacing factor of $s = 0.11$, and a negatively curved α-BBO lens was used in conjunction with a positive achromat to tailor the spacing factor to around $s = 0.04$.

A further consideration in using birefringent lenses for FINCH holography is the requirement in incoherent holography for a small optical path difference (OPD) between the light waves that are to interfere in the hologram. The difference must be less than the coherence length of the light, which is generally approximated as $\lambda^2/\Delta\lambda$, where λ is the centre wavelength and Δλ is the bandwidth. In the microscopy realm in which our work has been performed, the coherence length is on the order of 10 μm, at least an order of magnitude shorter than the lasers or monochromatic light to which previous interferometers with birefringent lenses have been restricted[15,16]. The optical path length OPL = $\sum_i d_i n_i$ is a function of the thicknesses d_i and refractive indices n_i of all of the media through which the light propagates. In any form of FINCH, the OPD between the two differentially focused beams has a geometric component due to the different physical paths that the light waves travel after exiting the differential focusing optic[7]; this component is less than the coherence length and thus does not prevent the waves from interfering. For the GRIN method the birefringence $|\Delta n| = |n_o - n_e|$ of the liquid crystal material in the GRIN lens is enough to cause an additional large OPD component that is greater than the coherence length, which must be compensated for by another optic if interference is to be observed[8]. A similar effect occurs in this case, in which the birefringent lens not only imparts different phase curvatures to the two waves through the two focal lengths f_{be} and f_{bo}, related to the curved surfaces of the lens, but also imparts an overall optical path difference ΔOPD between the two waves that is proportional to the thickness of the central cross-sectional part of the birefringent lens d_{BRL}:

$$\Delta\mathrm{OPD}=d_{\mathrm{BRL}}\Delta n \quad (5)$$

ΔOPD does not contribute to the desired geometric optical path difference, as there is no physical curvature in this part of the lens, and for a birefringent lens with thickness >1 mm and $\Delta n \cong 0.1$ it is far greater than the 10 μm coherence length and is thus sufficient to prevent interference from occurring. A correction similar to the GRIN method is made here, in which a compensating birefringent optical flat of a thickness that is equal to d_{BRL} and cut with the same orientation of its crystal axes is placed in the optical train with its extraordinary axis rotated by 90° in the transverse plane relative to the extraordinary axis of the birefringent lens, as in Fig. 2d. The wave that projects along the ordinary axis in the birefringent lens projects along the extraordinary axis of the compensating birefringent flat, and vice versa, so the non-spherical ΔOPD from the birefringent lens is cancelled by the compensating birefringent flat.

Results

Birefringent crystal lenses were constructed of naturally occurring calcite and synthetic α-BBO as described in the Methods and used to construct FINCH microscopes. Comparative results of experiments with calcite FINCH and our previous GRIN-based FINCH microscope set-up are shown in Fig. 3. The figures show the very significant advantages of birefringent calcite FINCH over GRIN-based FINCH. Note in Fig. 3a–c that the recorded 'raw' hologram from calcite FINCH has nearly perfectly spherical, well-modulated fringes —the ideal case for FINCH holography. This results in a complex hologram with a smooth, nearly featureless intensity profile (Fig. 3d,g) and a nearly perfect Fresnel (wrapped) phase pattern (Fig. 3e,h). The reconstructed spot (Fig. 3f,i) is free of artefacts. In contrast to this, the raw holograms from GRIN-based FINCH (Fig. 3j–l) are markedly asymmetrical, leading to a complex hologram with uneven features in the intensity profile (Fig. 3m,p) as well as phase distortions evident in the phase pattern (Fig. 3n,q). All of these factors affect the reconstructed spot, which shows significant sidebands (Fig. 3o,r). It should be noted that the differences in hologram diameter are caused by the fact that s of GRIN-based FINCH is about 0.03, while that of calcite FINCH is approximately 0.11, and that this along with the secondary relay of calcite FINCH, affects the size of the reconstructed spot, rendering that quantity alone insufficient for judging the performance of the birefringent lens relative to the GRIN lens. However, the improvements in the raw hologram symmetry and complex hologram intensity and phase are not dependent on s and clearly indicate the advantages of the birefringent lens over the GRIN lens in producing FINCH interference. Calcite is difficult to obtain in large, high-optical-quality pieces, and is also brittle and difficult to fabricate, thus it was necessary to use more readily available birefringent crystals to fabricate the FINCH interferometer lenses. Additional birefringent optics were made from α-BBO due to its temperature and environmental stability, as well as the fact that it can be grown in large single crystals with high optical quality.

Imaging of the US Air Force pattern with α-BBO-FINCH with a low-magnification, low-NA objective (×20, 0.75 NA) revealed a performance equal to earlier GRIN-based FINCH

(see Supplementary Information and Supplementary Fig. 1). Sub-resolution 110 nm fluorescent beads (Fig. 4) or component proteins of the Golgi apparatus in HeLa cells (Fig. 5), which require a resolving power greater than the Rayleigh limit, were imaged with high-magnification, high-NA objectives using α-BBO-FINCH. This was not possible using previous SLM- or GRIN-based FINCH systems. When the beads were imaged with α-BBO-FINCH using a Nikon ×60 1.49 NA total internal reflection fluorescence objective (in epifluorescence geometry), the α-BBO-FINCH measurements of the bead sizes averaged 149 ± 11 nm, significantly smaller than the 287 ± 20 nm average from the corresponding classical images of the same exact beads. These results are comparable to beads imaged at a shorter wavelength by another super-resolution technique[17]. To take our measurements, the beads were imaged as in the standard FINCH method. The reconstructed image stack surrounding the plane of focus was then deconvolved as described in the Methods. A random selection of 20 beads was made from various parts of the central 31 × 31 μm section of the best-focused reconstructed FINCH image, and the vertical and horizontal line profiles through the peak pixel of each image were fit to Gaussian functions. The average width of those functions was used as the bead size. The first 20 beads that were identified were measured without selection bias. The same beads simultaneously captured on the wide-field camera were then measured by the same method. Images of the measured beads and a section from the full images are shown in Fig. 4. To our knowledge these are the smallest objects that have been measured by any self-referenced holographic method, as well as the first demonstration of super-resolved self-referenced holographic imaging of any kind with a high-magnification, high-NA system. This was made possible by the high imaging quality of the distortion-free birefringent crystal lens incoherent interferometer that was incorporated into the FINCH system.

The real utility of a super-resolving microscope is the facile routine imaging of multiple fluorescently labelled biological samples to localize proteins and other substances in cells. A holographic method of viewing sub-resolution cellular structures without the need for labelling with fluorescent dyes has been presented[18], though it lacks the specificity that dyes impart. The FINCH microscope that incorporated the incoherent birefringent crystal lens interferometer was able to rapidly and readily obtain super-resolved images in cells of fluorescent proteins labelled with different fluorescent dyes. For example, we could readily discriminate individual sub-resolution protein components of the Golgi apparatus in HeLa cells. As shown in Fig. 5, three different proteins could be imaged in the same cells: stably expressed *trans*-Golgi marker GalT-GFP, *cis*-Golgi marker GM130 and TGN46 labelled correspondingly with DyLight549 and by DyLight647. The images clearly demonstrate each of the components closely but distinctly localized in the Golgi apparatus. Exposure time per hologram for each of three holograms per colour was 100 ms.

Our results were compared with those obtained with a leading commercial structured illumination (SIM) microscope. An example image from that microscope using the same fluorescent probes in HeLa cells is shown in Supplementary Fig. 2. The results with FINCH are more than comparable to those obtained with that instrument. However, the optimal results using the SIM microscope required 25 100 ms image captures per colour, while with FINCH, only three phase-shifted 100 ms image captures per colour were required. Furthermore with FINCH we were able to use a much simpler and dramatically less costly

objective and net FINCH exposure times were almost ten times shorter. Additionally, the FINCH calculation method is simpler and requires less stringent imaging conditions to avoid artefacts.

At present, FINCH requires three phase-shifted image captures per colour, and although this is still fast in comparison to SIM, and suggestive of the ability to image in live cells with minimal motion artefacts, there are potential opportunities to obtain high-resolution holographic images even faster without any electronic phase-shifting and with only one image capture. Some such possibilities include the use of compressive sensing to calculate the final images from a single captured hologram[19], as well as the simultaneous image capture schemes described previously[8]. Optimization of the image computation is expected to lead to much shorter than our current 9 s per colour channel computation time for a 40 μm square field imaged with a ×100 objective. Thus the development of the single-crystal birefringent lens for FINCH holographic imaging enables FINCH to reach its expected resolution with very-high-NA and high-power objectives. This is because aberrations in the hologram-forming elements have been eliminated by these non-quantized devices.

The new birefringent crystal lens interferometer is an inherently stably aligned all-optical, low-aberration system, which creates super-resolved self-interference holograms without the requirement for electrical control to create interference. These new crystal lens interferometers provide a variety of opportunities to create holographic images from a single hologram capture, obviating the need for electronic phase-shifting and thus potentially yielding an even simpler high-resolution, single-shot in-line optical system for incoherent holographic imaging. We anticipate that these birefringent lens interferometers may also be useful in a variety of other applications where classical two-beam interferometers are used.

Methods

Methods and any associated references are available in the online version of the paper.

Methods

Preparation and characterization of birefrigent lenses

Birefringent lenses and optical flats of calcite and of α-BBO were made by standard methods for the fabrication of optical glass components, with their extraordinary axes lying in the plane orthogonal to the direction of light propagation through the optic. Calcite optics were 2.6 mm thick at their centres and α-BBO optics were 3 mm thick at their centres. The calcite lens was plano-convex (positive) with R_{eff} = 127 mm, while the α-BBO lens was plano-concave (negative) with R_{eff} = −545 mm. The negative effective curvature of the α-BBO lens was selected to reduce the spacing factor of the holographic system from that of a pure birefringent lens system by combining it with a classical glass lens as discussed in the Supplementary Information.

Microscope configurations with calcite or α-BBO birefrigent lens interferometers

FINCH microscopes with calcite or α-BBO lens interferometers were assembled with these lenses and were similar in design to that of a GRIN-based FINCH microscope reported in

ref. 8 and depicted in Fig. 1, with the following exceptions: in calcite FINCH, the calcite lens was substituted for the GRIN/glass lens combination, and a finite conjugate relay system of a 60 mm achromatic lens (Thorlabs AC254-060-A) followed by a 200 mm achromat (Thorlabs AC254-200-A) was used to image the hologram plane onto the camera chip; in α-BBO FINCH the α-BBO lens and a 250 mm achromat (Thorlabs AC254-250-A) were substituted for the GRIN/glass lens combination, and a Thorlabs variable waveplate (LCC1223-A) was used instead of a similar device from Citizen Corp to effect the holographic phase shift. In both birefringent lens FINCH microscopes, birefringent flats made from the same material as the birefringent lens was installed in the optical train after the birefringent lens in the 90° rotated orientation. Because flexibility in the placement of the optics was necessary during this development, a custom microscope configuration was constructed rather than trying to adapt to existing microscopes. In the future it may be possible to adapt existing microscopes for FINCH imaging using these birefringent lenses.

Hologram recording and calculations

Calcite FINCH was used to benchmark the performance of a birefringent lens against that of GRIN-based FINCH operating on a theoretically perfect model beam. The model beam was a 633 nm randomly polarized laser (Thorlabs HNL020R) that was focused into a single-mode fibre and re-collimated on exiting the fibre to a collimated beam of ~15 mm diameter. This beam was used as a substitute for a randomly polarized sub-resolution emitter at the focal plane of an infinity objective, that is, a point spread function (PSF) object. The actual microscope objective was removed from calcite FINCH or GRIN-based FINCH and the laser beam was directed down the optical axis of the microscope. Three phase-shifted holograms were collected in each microscope and processed following published procedures[3,9,11]. α-BBO FINCH was used to image fluorescent model objects with low- and high-power objectives. A Cy3 fluorescent USAF pattern was imaged with a ×20 0.75 NA Nikon objective (as used in refs 5,6,8,10,11), while a sample of 110 nm Tetraspec beads (Invitrogen T14792) was imaged using a ×60 Nikon 1.49 NA TIRF objective with Cy3 excitation and emission filters (Semrock Cy3-4040C-000-ZERO) with excitation light provided by an 89 North Photofluor light source. For the triple dye fluorescently labelled HeLa cell experiment a ×100 Nikon 1.4 NA objective was used and excitation light was provided by an 89 North LDI scrambled laser source with a Chroma quad band filter set. Selection of the 465, 555 or 640 nm laser line provided excitation and specific emission for GFP, DyLight549 (similar to cy3) or DyLight647 (similar to cy5) respectively without having to move any filters. We confirmed image registration of these multiple emission wavelengths using the multicoloured Tetraspec fluorescent beads. The index-matching oil was Cargille type DF or type HF (n = 1.515 for both). For the ×20 objective, the FINCH image pixel size was 187 nm, for the ×60 objective it was 62 nm and for the ×100 objective it was 37 nm. With the object at the focal plane of the objective, three phase-shifted holograms were recorded on a sCMOS camera (pco.edge 4.2) and processed following the published procedures[3,11,14] to create the complex hologram and stacks of reconstructed images representing the object travelling through the focus of the objective. Simultaneously, conventional focused images were recorded on a separate sCMOS camera from the s polarization rejected from the FINCH optical train using a 300 mm achromat (Thorlabs AC254-300-A) similar to ref. 8. The reconstruction stacks of the USAF pattern were not

processed further. The reconstruction stacks (100 nm steps between 1 μm above and 1 μm below the objective focal plane) of the 110 nm beads taken with the ×60 and the HeLa cells taken with the ×100 objective were deconvolved with a GPU-accelerated blind routine (Microvolution, Inc.) with maximum entropy regularization and a starting PSF calculated from simulated perfect holograms of a sub-resolution emitter. The best-focused images were selected from the stacks for further analysis.

Fluorescently labelled Golgi proteins

HeLa GalT-GFP stably transfected cells grown on 12 mm glass coverslips (#1.5, 0.17 mm thickness) were fixed and stained as described previously[20]. In short, cells were fixed in 4% paraformaldehyde (16% stock solution diluted in Dulbecco's PBS (DPBS); Electron Microscopy Sciences). Cells were then treated with 0.1% Triton X-100 for 1 min and with 50 mM ammonium chloride for 5 min. Cells were washed with DPBS and blocked twice for 10 min with 1% BSA, 0.1% saponin in DPBS. Cells then were incubated for 1 h with primary mouse monoclonal anti-GM130 (Life Technologies) and sheep anti-TGN-46 (AbD Serotec) antibodies diluted in antibody buffer (1% cold fish gelatin, 0.1% saponin in DPBS) at roomtemperature. Cells were washed four times with DPBS and incubated for 30 min with fluorescently tagged secondary antibody (donkey-anti-mouse- DyLight647 and donkey-anti-sheep-DyLight549, Jackson ImmunoResearch) in antibody buffer at room temperature. Coverslips were washed four times with DPBS, rinsed with ddH_2O, and mounted on glass microscope slides using Prolong Gold antifade reagent (Life Technologies).

Supplementary Material

Refer to Web version on PubMed Central for supplementary material.

Acknowledgments

This work was supported by CellOptic, Inc. and the National Institutes of Health under National Cancer Institute Award Number R44CA192299 and National Institute of General Medical Sciences Award Number U54GM105814. The content is solely the responsibility of the authors and does not necessarily represent the official views of the National Institutes of Health. Patents have been applied for. We thank M. Bruce and M. Butte for assistance with the deconvolution.

References

1. Gabor D. A new microscopic principle. Nature. 1948; 161:777–778. [PubMed: 18860291]
2. Poon T-C, et al. Three-dimensional fluorescence microscopy by optical scanning holography. Opt. Eng. 1995; 34:1338–1344.
3. Rosen J, Brooker G. Digital spatially incoherent Fresnel holography. Opt. Lett. 2007; 32:912–914. [PubMed: 17375151]
4. Rosen J, Brooker G. Non-scanning motionless fluorescence three-dimensional holographic microscopy. Nat. Photon. 2008; 2:190–195.
5. Brooker G, Siegel N, Wang V, Rosen J. Optimal resolution in Fresnel incoherent correlation holographic fluorescence microscopy. Opt. Express. 2011; 19:5047–5062. [PubMed: 21445140]
6. Rosen J, Siegel N, Brooker G. Theoretical and experimental demonstration of resolution beyond the Rayleigh limit by FINCH fluorescence microscopic imaging. Opt. Express. 2011; 19:26249–26268. [PubMed: 22274210]

7. Katz B, Rosen J, Kelner R, Brooker G. Enhanced resolution and throughput of Fresnel incoherent correlation holography (FINCH) using dual diffractive lenses on a spatial light modulator (SLM). Opt. Express. 2012; 20:9109–9121. [PubMed: 22513622]
8. Brooker G, et al. In-line FINCH super resolution digital holographic fluorescence microscopy using a high efficiency transmission liquid crystal GRIN lens. Opt. Lett. 2013; 38:5264–5267. [PubMed: 24322233]
9. Siegel N, Brooker G. Improved axial resolution of FINCH fluorescence microscopy when combined with spinning disk confocal microscopy. Opt. Express. 2014; 22:22298–22307. [PubMed: 25321701]
10. Siegel N, Rosen J, Brooker G. Reconstruction of objects above and below the objective focal plane with dimensional fidelity by FINCH fluorescence microscopy. Opt. Express. 2012; 20:19822–19835. [PubMed: 23037035]
11. Siegel N, Rosen J, Brooker G. Faithful reconstruction of digital holograms captured by FINCH using a Hamming window function in the Fresnel propagation. Opt. Lett. 2013; 38:3922–3925. [PubMed: 24081089]
12. Rosen J, Brooker G. Fluorescence incoherent color holography. Opt. Express. 2007; 15:2244–2250. [PubMed: 19532459]
13. Kim MK. Adaptive optics by incoherent digital holography. Opt. Lett. 2012; 37:2694. [PubMed: 22743498]
14. Yamaguchi I, Zhang T. Phase-shifting digital holography. Opt. Lett. 1997; 22:1268–1270. [PubMed: 18185816]
15. Dyson J. Common-path interferometer for testing purposes. J. Opt. Soc. Am. A. 1957; 47:386–390.
16. Goto K, Sasaki M, Okuma S, Hane K. A double-focus lens interferometer for scanning force microscopy. Rev. Sci. Instrum. 1995; 66:3182–3185.
17. York AG, et al. Instant super-resolution imaging in live cells and embryos via analog image processing. Nat. Methods. 2013; 10:1122–1126. [PubMed: 24097271]
18. Cotte Y, et al. Marker-free phase nanoscopy. Nat. Photon. 2013; 7:113–117.
19. Weng J, Clark DC, Kim MK. Compressive sensing sectional imaging for single-shot in-line self-interference incoherent holography. Opt. Commun. 2016; 366:88–93.

References

20. Pokrovskaya ID, et al. Conserved oligomeric Golgi complex specifically regulates the maintenance of Golgi glycosylation machinery. Glycobiology. 2011; 21:1554–1569. [PubMed: 21421995]

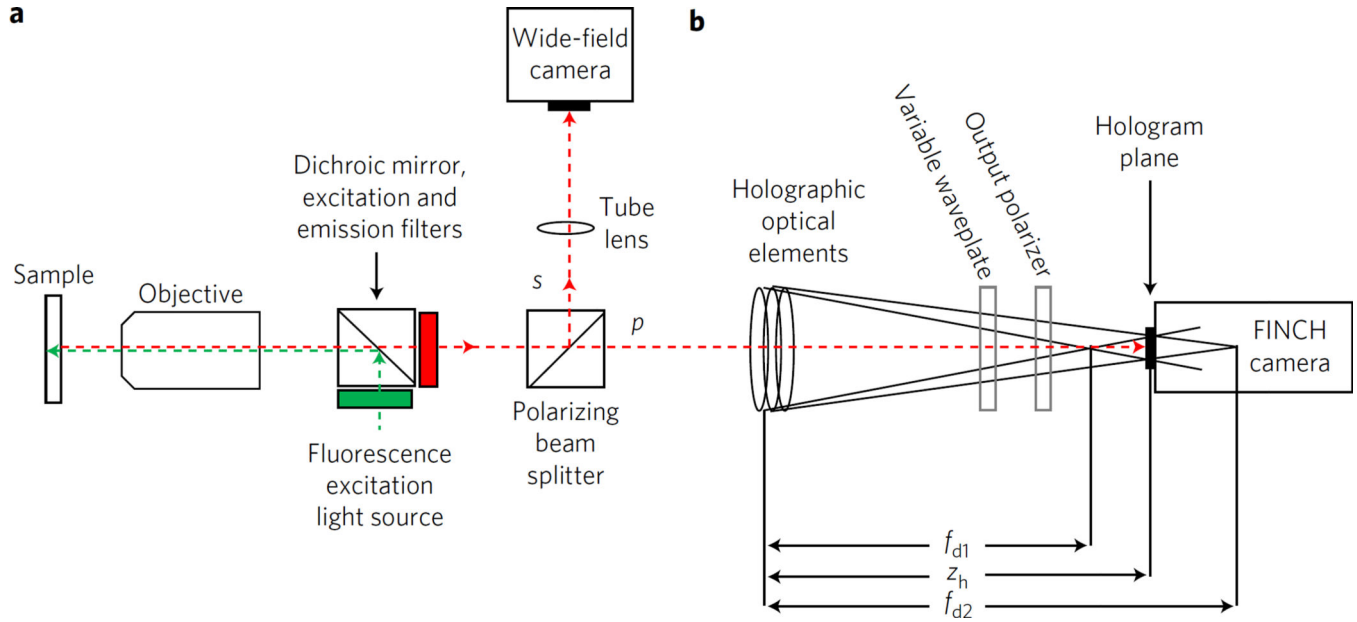

Figure 1. Conceptual schematic of a FINCH microscope

a, Fluorescent light emitted from a sample passes through an infinity-corrected objective, and is split into two polarized beams. The s polarization image component passes through a microscope tube lens and is captured on the wide-field camera as in a classical microscope. **b**, The beam is split into two orthogonally polarized beams typical of a FINCH hologram-forming system configured with SLM-based or GRIN-based lenses or the new birefringent crystal lens-based interferometer. The p polarization is directed through these optical elements, the two coincident beams interfere, creating holograms that are captured on the FINCH camera. The phase of the hologram can be changed by an optional polarization-sensitive variable waveplate if the phase-shifting holographic method is used, as was the case in the present experiments. The 4F relay system between **a** and **b** is not shown for simplicity.

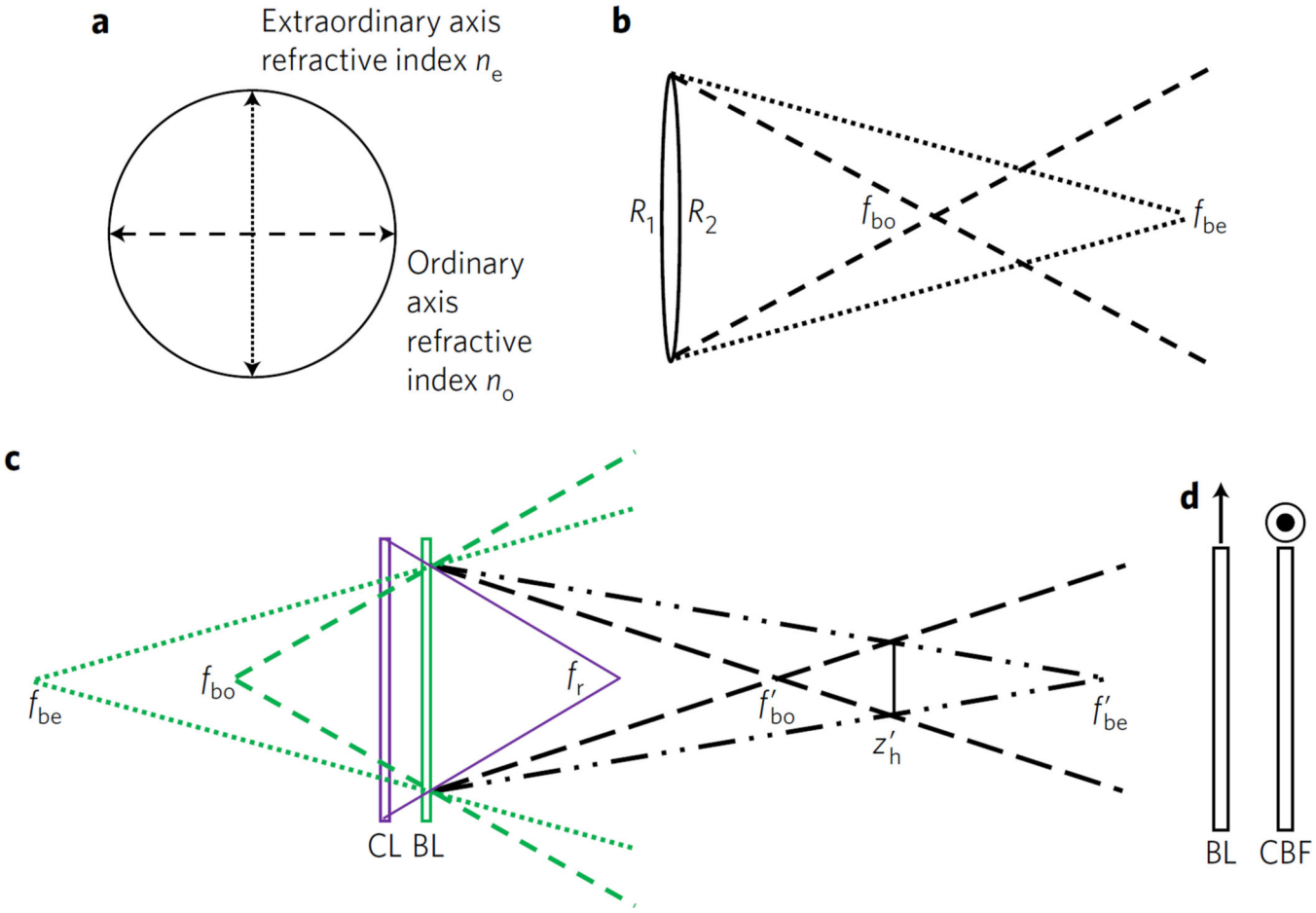

Figure 2. Optical arrangement of birefringent lens incoherent interferometers

a, Lateral view of a birefringent spherical lens depicting the orientation of the crystal ordinary and extraordinary refractive indices in the plane of the lens. **b**, The ordinary and extraordinary focal lengths f_{bo} and f_{be} of a birefringent crystal convergent lens. **c**, Combination of a classical positive non-birefringent lens (CL) with a negative birefringent lens (BL) to produce combined focal and hologram planes as in the Supplementary equations (3) and (5) and the accompanying explanations. Note that other combinations are possible as well. **d**, Combination of a BL with a birefringent compensating flat (CBF) to reduce the overall OPD encountered by the light propagating through the interferometer. The orientations of the extraordinary axes of the birefringent lens and the compensating flat are indicated by the arrow and target, representing in the plane of the paper and orthogonal axis, respectively.

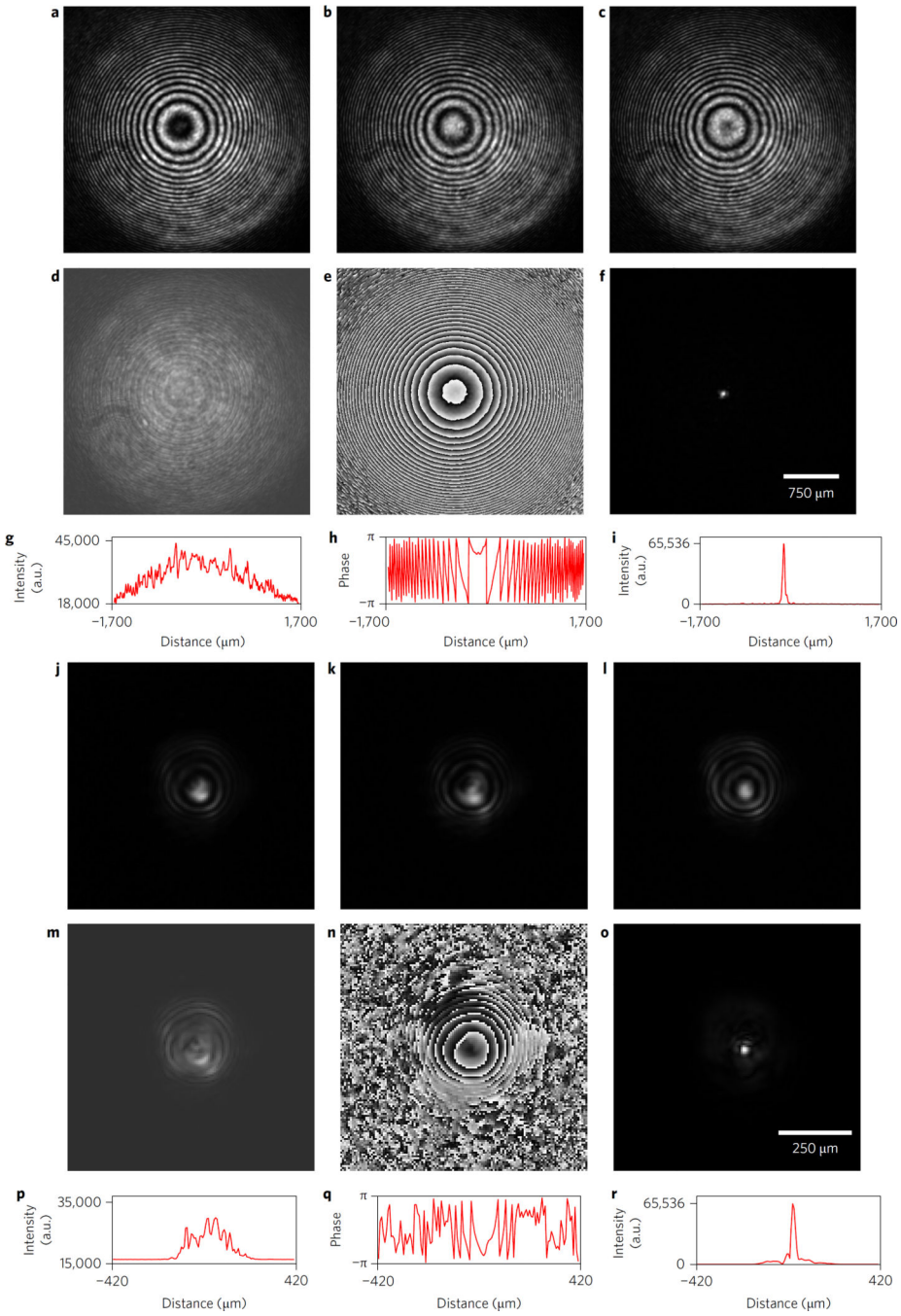

Figure 3. Holograms from a birefringent lens-based calcite and GRIN lens FINCH system after expanded laser beam illumination

a–i, Calcite FINCH system. **j–r**, Comparison GRIN FINCH system. **a–c,j–l**, Three phase-shifted raw holograms. **d,e,m,n**, Calcite FINCH (**d,e**) and GRIN FINCH (**m,n**) complex hologram amplitude and phase, respectively. **f**, Reconstructed point from calcite FINCH. **o**, Reconstructed point from GRIN FINCH. **g–i,p–r**, Horizontal line profiles through the middle of the amplitude, phase and reconstructed spots for calcite FINCH (**g–i**) and for GRIN FINCH (**p–r**).

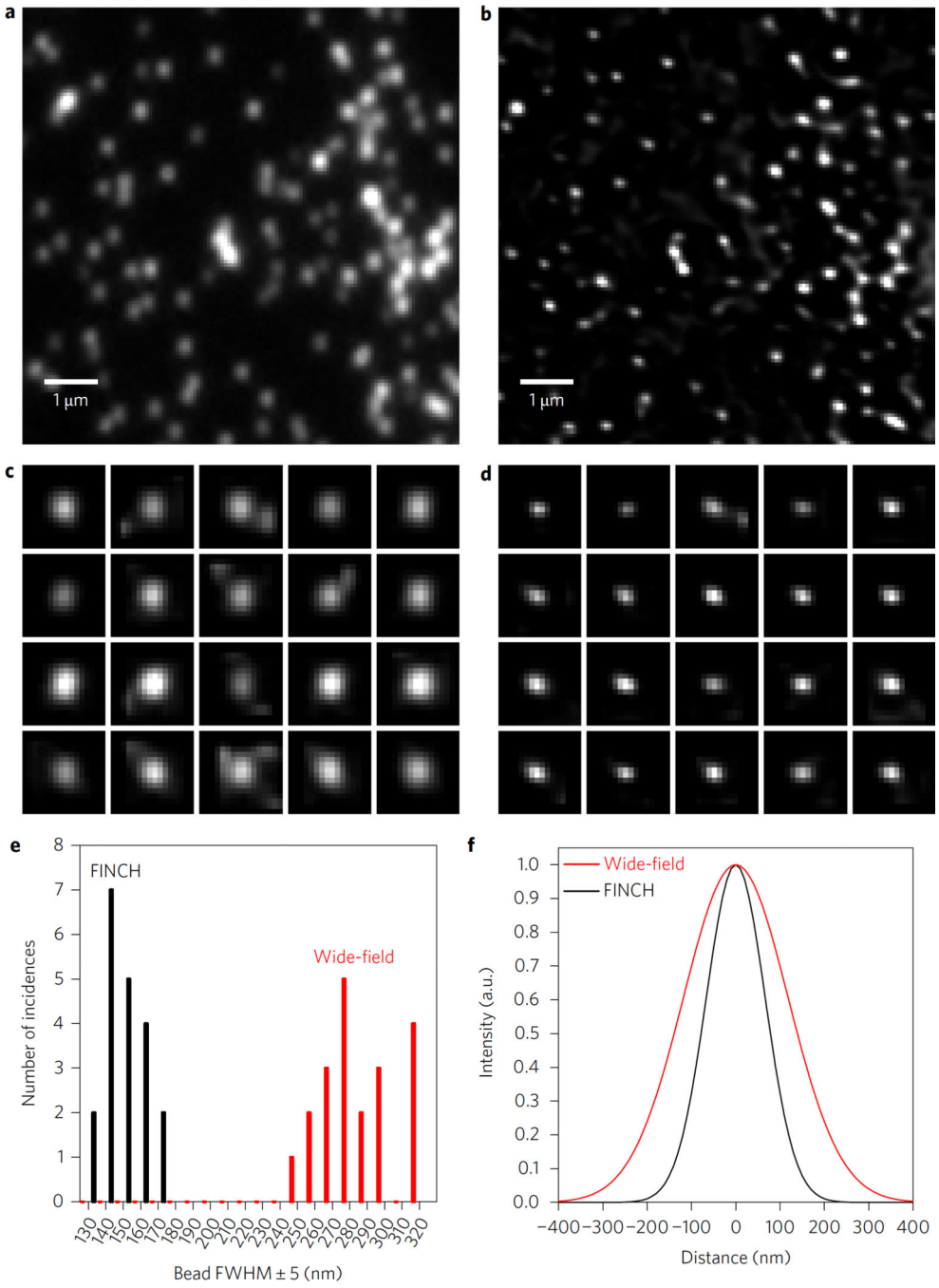

Figure 4. Resolution comparison of wide-field and α-BBO FINCH imaging of fluorescent beads

a,b, 8 × 8 μm^2 zoomed selections of 110 nm fluorescent beads for resolution comparison of the same area between wide-field fluorescence (**a**) and α-BBO-FINCH (**b**) images. The full fields were 62 × 62 μm^2. **c,d**, 1 μm^2 zoomed images of the same randomly selected beads from **a** and **b**, respectively. The beads in the respective parts of **c** and **d** are the same. **e**, A histogram of full-width at half-maximum (FWHM) size distributions among the 20 beads that were measured in **c,d**, showing the approximately twofold reduction in FWHM by FINCH. **f**, Plots depicting the average FWHM sizes of the 110 nm beads as measured by

wide-field fluorescence and α-BBO-FINCH microscopy, with normalized Gaussian functions of the average width measured from the 20 selected beads.

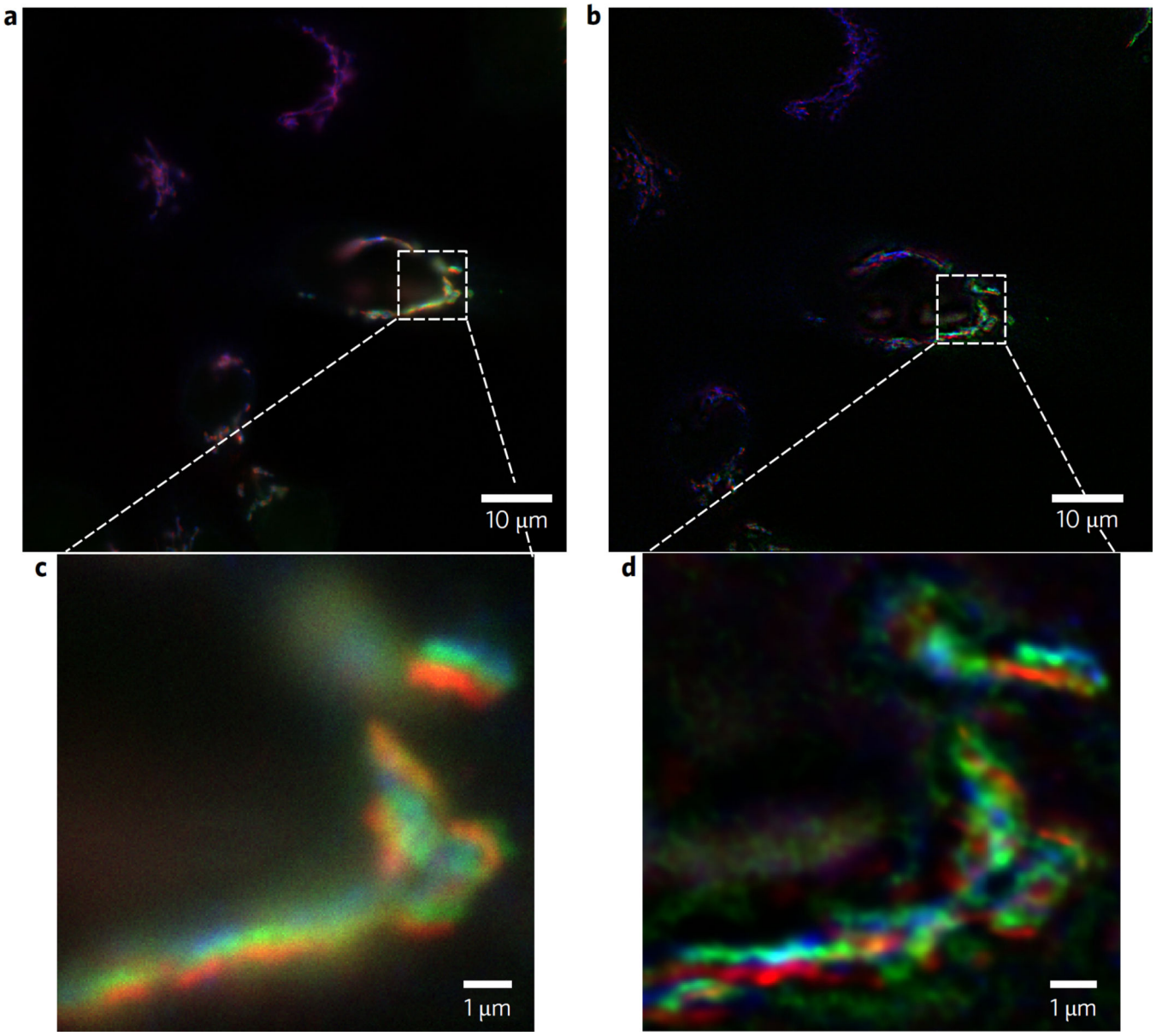

Figure 5. Comparative imaging of three different Golgi apparatus proteins in HeLa cells by wide-field and α-BBO FINCH

a,b, Wide-field (**a**) and FINCH (**b**) images of the Golgi apparatus proteins labelled with GalT-GFP (green), and two other Golgi proteins TGN46 and GM130 immunolabelled and respectively stained with DyLight549 (blue) and DyLight647 (red). The FINCH image was obtained after three holograms per colour (100 ms capture time per hologram) were captured at the excitation wavelength for each dye and the holograms were processed by Fresnel propagation and deconvolution as described. **c,d**, Corresponding enlarged 10 μm^2 selections. A Nikon × 100 1.4 NA Plan-Achromat objective was used.